PERGAMON

Acta mater. Vol. 47, No. 18, pp. 4653–4664, 1999

Printed in Great Britain
PII: S1359-6454(99)00312-2
1359-6454/99 $20.00 + 0.00

THE ROLE OF ADHESION IN CONTACT FATIGUE

A. E. GIANNAKOPOULOS, T. A. VENKATESH, T. C. LINDLEY† and S. SURESH‡

Department of Materials Science and Engineering, Massachusetts Institute of Technology, Cambridge, MA 02139, U.S.A.

(Received 26 May 1999; accepted in revised form 12 August 1999)

Abstract—By incorporating the effects of interfacial adhesion in the mechanics of rounded contact between two bodies, a new approach is proposed for the quantitative analysis of a wide variety of contact fatigue situations involving cyclic normal, tangential or torsional loading. In this method, conditions of "strong" and "weak" adhesion are identified by relating contact mechanics and fracture mechanics theories. Invoking the notion that for strong and weak adhesive contact, a square-root stress singularity exists at the rounded contact edge or at the stick–slip boundary, respectively, mode I, II or III stress intensity factors are obtained for normal, sliding and torsional contact loading, accordingly. A comparison of the cyclic variations in local stress intensity factors with the threshold stress intensity factor range for the onset of fatigue crack growth then provides critical conditions for crack initiation in contact fatigue. It is shown that the location of crack initiation within the contact area and the initial direction of crack growth from the contact surface into the substrate can be quantitatively determined by this approach. This method obviates the need for the assumption of an artifical length scale, i.e. the initial crack size, in the use of known fracture mechanics concepts for the analyses of complex contact fatigue situations involving rounded contact edges. Predictions of the present approach are compared with a wide variety of experimental observations.

Keywords: Adhesion; Fracture; Fatigue; Wear; Surfaces and interfaces

1. INTRODUCTION

Functional structures, at macro or micro size-scales, by design or default, involve contact between similar or dissimilar materials, under static or cyclic loading conditions, in a passive or aggressive, thermo-chemical environment. Consequently, in the most general case, different aspects of contact such as material properties, interface chemistry and contact mechanics can independently or interdependently influence the overall mechanical behavior of the contacting system.

In most cases, the bulk mechanical behavior of the contacting system is characterized by a macroscopic continuum level analysis that evaluates the uncoupled mechanics response [1]. However, a more complete analysis requires a consideration of the microscopic or atomic structure where coupled interactions at the contact interface become significant. These are typically analyzed within the framework of surface thermodynamics by recognizing that contacting surfaces are subject to short-range interatomic forces such as the van der Waals forces. Consequently, spontaneous adhesion leading to the formation of a low energy interface reduces the total energy of the system, while elastic deformation across the interface that accomodates adhesion leads to an increase in the potential energy of the system. The resulting thermodynamic equilibrium and extent of adhesion is then determined by the relative dominance of these competing phenomena.

For monotonic contact loading, adhesion has been well documented analytically and experimentally under normal loads [1–5], and to a lesser extent under tangential loads [6]. For cyclic loading, a number of experimental studies have investigated adhesion in a variety of materials — metals [7, 8], glasses [9], and polymers [10], for different surface and environmental conditions [11, 12], temperatures [13], hardness [8], and fatigue cycles [14].

Theoretical work has demonstrated that under monotonic compressive loading of the contact interface, adhesion induces tensile square-root singular stress fields at the contact edges [2, 3]. However, connections to contact fatigue experiments specifically aimed at correlations between adhesion and fatigue crack initiation have not been established.

The objectives of the present work are, therefore, to develop and experimentally validate a general continuum level mechanics model that incorporates work of adhesion, material elastic properties, and contact loads, for predicting key features of contact fatigue crack initiation (thresholds for the onset of

†Permanent address: Department of Materials, Imperial College of Science, Technology and Medicine, Prince Consort Road, London SW7 2BP, U.K.

‡To whom all correspondence should be addressed.

cracking, location of cracking, and initial orientation of the crack plane with respect to the contact surface) for a variety of loading conditions (cyclic mode I or steady mode I with cyclic mode II or cyclic mode III) and contact geometry (sphere or cylinder on a planar substrate).

This paper addresses the following key issues of contact mechanics and contact fatigue.

First, the present work extends the crack analogue methodology developed earlier [15] for the contact between a sharp-edged pad and a planar substrate, where stress singularities are introduced by the sharp cornered geometry. We now investigate the more general case of rounded contacts where stress singularities are induced by adhesion† and thus present a universal methodology that enables analysis of a variety of contact problems from those due to fretting fatigue in large-scale structures to contact fatigue in micro-scale devices, with adhesive or non-adhesive, sharp or rounded geometries.

Second, as the adhesion-induced, square-root singular stress fields are amenable for analysis within the framework of a "crack analogue" [15], the pre-existing long crack introduced by the contact circumvents "length scale" problems inherent in the modeling of crack initiation based on conventional fracture mechanics [16], or small crack growth based on initial dislocation distributions [17].

Third, under conditions of small-scale yielding, the effects of static and/or oscillatory bulk stresses (i.e. residual stresses induced by surface treatments such as shot-peening or laser shock-peening, or far-field applied stresses acting parallel to the contact surface) on contact fatigue crack initiation can also be analyzed by recognizing that these are analogous to the *T*-stresses present in a simple linear elastic fatigue–fracture formulation.

Fourth, all previous analyses which are based on stress-based approaches to fatigue at critical points (such as those using elastic stress fields of a sphere on a flat plane [18] in combination with a variety of fatigue strain-based, multiaxial criteria for endurance limits [19–22], predict contact fatigue cracking to initiate at the contact perimeter. This prediction is contrary to many experimental results which clearly indicate that cracking could initiate at either the contact perimeter or the stick–slip boundary. The present analysis, though an examination of the work of adhesion *via-á-vis* the crack driving force arising from the contact loads, leads to a novel classification whereby cases of strong and weak adhesion are recognized unambiguously‡. Thus, the crack initiation location (contact perimeter for strong adhesion and the stick–slip boundary for weak adhesion) can be predicted without uncertainty.

Fifth, the present methodology conceptually facilitates the incorporation of known effects of surface conditions, environment, hardness, and temperature on adhesion, through a simple modification of the work of adhesion.

The paper is arranged in the following sequence. The mechanics of adhesive contacts for a variety of monotonic loading conditions are reviewed in Section 2. The contact mechanics of cyclic loading for three-dimensional, spherical, adhesive contacts are analyzed in Section 3. The results of the adhesion model for cyclic loading for two-dimensional, cylindrical contacts are presented in Section 4. The range of applicability of the adhesion model as well as its significance and limitations are discussed in Section 5. Available experimental results for different material systems and loading configurations are compared to model predictions in Section 6. Finally, the paper concludes with a summary of results and potential palliatives for contact fatigue from the perspective of the adhesion model in Section 7.

2. MECHANICS OF STATIC ADHESIVE CONTACT

Consider a sphere of diameter, D, elastic modulus, E, and Poisson ratio, ν, contacting the planar surface of a large substrate of similar material, Fig. 1(a), with r and z being the global radial and depth coordinates attached to the center of the contact circle. Three loading conditions are considered as follows.

2.1. Normal loading

For elastic, monotonic loading from zero to $P_{\max}$ (>0), under non-adhesive conditions, the contact stress field is non-singular [Fig. 1(b)] and the maximum contact radius, a_0, is given as [1]

$$a_0 = \left[\frac{3D(1-\nu^2)}{4E}P_{\max}\right]^{1/3}. \tag{1}$$

Under adhesive conditions, when two surfaces with surface energies γ_1 and γ_2 adhere to form a new interface of lower energy, γ_{12}, the corresponding work of adhesion is defined as, $w=(\gamma_1+\gamma_2-\gamma_{12})\geq 0$. For two contacting solids with the same elastic properties, which are presently considered, $w=2\gamma_1$. For metals, $w\approx 1$ N/m [23].

The short-range forces of attraction that promote adhesion effectively increase the contact load across the interface and thus increase the contact radius, $a_{\max}$ [Fig. 1(c)], to the one given as

†The adhesion induced stress singularities are not expected to modify the geometry induced stress singularities in the case of sharp edged contacts.

‡The conditions of strong and weak adhesion can conceptually be visualized as being analogous, respectively, to the concepts of "static" and "dynamic" friction when the interfacial slip behavior across two contacting surfaces is considered.

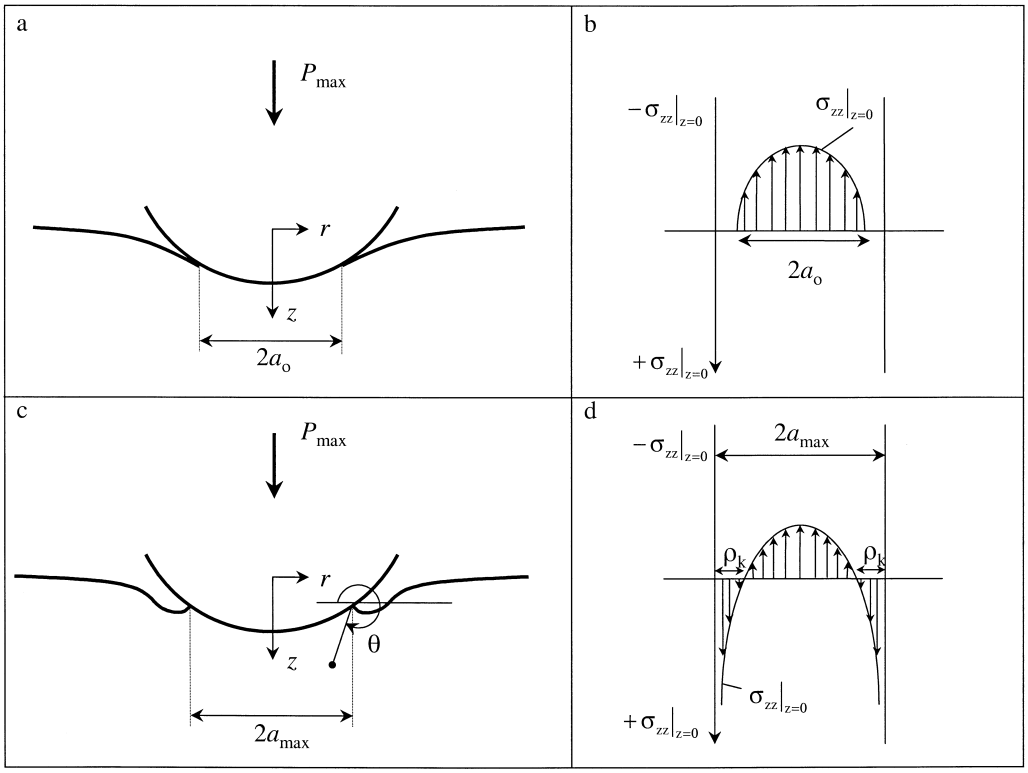

Fig. 1. Schematics illustrating: (a) non-adhesive contacts and (b) the corresponding non-singular contact stress field; (c) adhesive contacts and (d) the corresponding stress field exhibiting tensile square-root singularity.

$$a_{max} = \left[\frac{3D(1-\nu^2)}{4E} \left(P_{max} + \frac{3\pi Dw}{2} + \sqrt{3\pi Dw P_{max} + \left(\frac{3\pi Dw}{2}\right)^2} \right) \right]^{1/3}. \quad (2)$$

The apparent load, P^*_{max}, required to maintain the same contact radius, a_{max}, without adhesion is given by Hertzian analysis [1]

$$P^*_{max} = \frac{4Ea^3_{max}}{3(1-\nu^2)D}. \quad (3)$$

Unlike the non-adhesive case (Fig. 2), the adhesive contact produces a tensile, square-root singular stress field [24] which is asymptotically equal to the mode I crack field at the contact perimeter (Fig. 1(d)). With ρ and θ as the local polar coordinates at the contact perimeter, ϕ the angular circumferential coordinate, and T_{rr} and $T_{\phi\phi}$ as the non-singular stress terms in the radial and circumferential directions, the asymptotic stress field is given by [24]

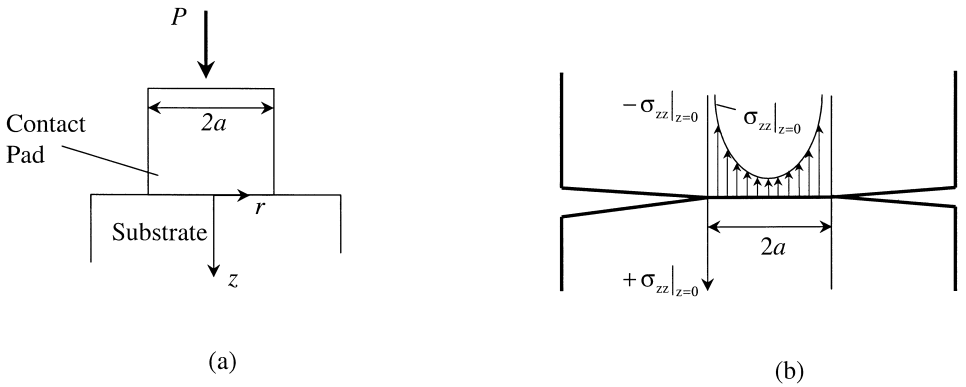

Fig. 2. Schematics illustrating: (a) sharp-edged, non-adhesive contact and (b) the corresponding crack analogue exhibiting compressive stress singularity.

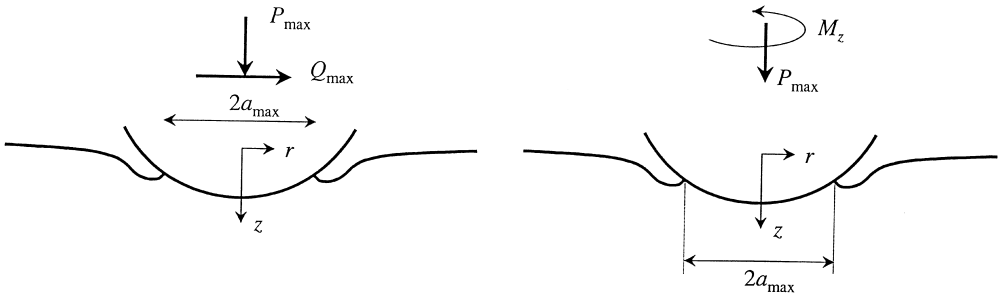

(a) (b)

Fig. 3. Schematics illustrating: (a) tangential loading and (b) torsional loading of adhesive, spherical contacts.

$$\sigma_{rr}^{nor} = \frac{K_1}{\sqrt{2\pi\rho}} \cos\frac{\theta}{2}\left(1 - \sin\frac{\theta}{2}\sin\frac{3\theta}{2}\right) + T_{rr} \tag{4a}$$

$$\sigma_{zz}^{nor} = \frac{K_1}{\sqrt{2\pi\rho}} \cos\frac{\theta}{2}\left(1 + \sin\frac{\theta}{2}\sin\frac{3\theta}{2}\right) \tag{4b}$$

$$\sigma_{rz}^{nor} = \frac{K_1}{\sqrt{2\pi\rho}} \cos\frac{\theta}{2}\left(\sin\frac{\theta}{2}\cos\frac{3\theta}{2}\right) \tag{4c}$$

$$\sigma_{\phi\phi}^{nor} = \nu(\sigma_{rr}^{nor} - T_{rr} + \sigma_{zz}^{nor}) + T_{\phi\phi}. \tag{4d}$$

The corresponding tensile stress intensity factor, K_1, is given as [25, 26]

$$K_1 = \frac{P^* - P_{max}}{2a_{max}\sqrt{\pi a_{max}}}. \tag{5}$$

The size of the K-dominance around the contact perimeter, ρ_k, is identified by the nodal positions in the stress field [Fig. 1(d)] and is given by

$$\rho_k = \frac{D}{4}\sqrt{\frac{2(1-\nu^2)\pi w}{Ea_{max}}}. \tag{6}$$

The associated energy release rate can be identified as $(1-\nu^2)K_1^2/E$†. The maximum non-singular stresses in the radial and circumferential directions due to contact at maximum load are given by

$$\max T_{rr} = -\max T_{\phi\phi} = \max T = \frac{(1-2\nu)P_{max}^*}{2\pi a_{max}^2}. \tag{7}$$

2.2. Combined normal and tangential loading

For elastic, monotonic, tangential loading from zero to Q_{max} (>0), under a constant normal load, P_{max}, an adhesion-induced, square-root singular stress field [6] is obtained at the contact perimeter (Fig. 3(a)). The mode II field, at the leading and the trailing edges‡, can be expressed as [15]

$$\sigma_{rr}^{tan} = \frac{K_{II}}{\sqrt{2\pi\rho}}\left(-\sin\frac{\theta}{2}\right)\left(2 + \cos\frac{\theta}{2}\cos\frac{3\theta}{2}\right) \tag{8a}$$

$$\sigma_{zz}^{tan} = \frac{K_{II}}{\sqrt{2\pi\rho}} \sin\frac{\theta}{2}\cos\frac{\theta}{2}\sin\frac{3\theta}{2} \tag{8b}$$

$$\sigma_{rz}^{tan} = \frac{K_{II}}{\sqrt{2\pi\rho}} \cos\frac{\theta}{2}\left(1 - \sin\frac{\theta}{2}\sin\frac{3\theta}{2}\right) \tag{8c}$$

$$\sigma_{\theta\theta}^{tan} = \nu(\sigma_{rr}^{tan} + \sigma_{zz}^{tan}) \tag{8d}$$

where the mode II stress intensity factor, K_{II}, is given as

$$K_{II} = \frac{Q_{max}}{2a_{max}\sqrt{\pi a_{max}}}. \tag{9}$$

The maximum T-stresses due to contact are obtained at the maximum tangential load and are given as

†(a) For contacting surfaces of different diameters, D can be replaced by $D_1D_2/(D_1+D_2)$, where the indices 1 and 2 refer to the contacting bodies 1 and 2. (b) For contact involving elastically dissimilar materials, $(1-\nu^2)/E$ can be replaced by $\{[(1-\nu_1^2)/E_1 + (1-\nu_2^2)/E_2]\}/2$ and the energy release rate relations are preserved. However, the form of the stress intensity factor remains invariant only if the stress fields are square-root singular for which the second Dundurs' parameter, $\beta = 0$ [27], i.e.

$$\frac{E_2(1+\nu_1)(1-2\nu_1) - E_1(1+\nu_2)(1-2\nu_2)}{E_2(1-\nu_1^2) + E_1(1-\nu_2^2)} = 0.$$

‡In general, a mixed mode II/III field is obtained along the contact perimeter with the corresponding stress intensity factors being:

$$K_{II} = \frac{Q_{max}\cos\phi}{2a_{max}\sqrt{a_{max}}}, \quad K_{III} = \frac{Q_{max}\sin\phi}{2a_{max}\sqrt{a_{max}}}$$

where ϕ is the angle between the radius vector at the peripheral point and the direction of Q_{max} [29].

$$\max\ T_{rr} = \frac{P^*_{\max}}{2\pi a^2_{\max}}\left[(1-2\nu) + \frac{3\mu\pi(4+\nu)}{8}\right] \quad (10a)$$

$$\max\ T_{\phi\phi} = -\frac{P^*_{\max}}{2\pi a^2_{\max}}\left[(1-2\nu) - \frac{9\mu\pi\nu}{8}\right]. \quad (10b)$$

2.3. Combined normal and torsional loading

For elastic, monotonic, torsional loading from zero to M_z (>0) (Fig. 3(b)), under a constant normal load, $P_{\max}$, the adhesive asymptotic stress field due to torsional loading†, is square-root singular at the contact perimeter [28]:

$$\sigma^{\text{tor}}_{rz} = \frac{K_{\text{III}}}{\sqrt{2\pi\rho}}\ \sin\ \frac{\theta}{2}, \quad \sigma^{\text{tor}}_{\theta z} = \frac{K_{\text{III}}}{\sqrt{2\pi\rho}}\ \cos\ \frac{\theta}{2} \quad (11)$$

with the mode III stress intensity factor, K_{III}, given as

$$K_{\text{III}} = \sigma^{\text{tor}}_{rz}\sqrt{2\pi(a_{\max} - r)} = \frac{3M_z}{4a^2_{\max}\sqrt{\pi a_{\max}}}. \quad (12)$$

The maximum energy release rate, max G, is related to the mode I and III stress intensity factors as

$$\max\ G = \frac{K^2_{\text{III}}(1+\nu)}{E} + \frac{K^2_{\text{I}}(1-\nu^2)}{E} \quad (13)$$

where K_{III} is given by equation (24) and K_{I} is given by equation (26). The mode III fields do not produce any T-stresses.

3. MECHANICS OF CYCLIC ADHESIVE CONTACT

3.1. Model assumptions

In modeling adhesive contacts under cyclic loading conditions, we invoke the following assumptions.

1. Materials are homogeneous, isotropic and linear elastic.
2. In order to keep the analysis simple and to avoid complications from elastic mismatch of the contacting bodies and from the strong nonlinear effects of contact geometry, only the sphere or cylinder on flat surface of similar materials is analyzed. To avoid microstructural scale effects, the contact area is assumed to cover at least several grains of the material.
3. For ideal contact conditions characterized by clean, smooth surfaces under inert atmospheres, a direct relationship between adhesion and friction can be obtained [30–32]. However, under real, ambient, atmospheric conditions, where the contacting surfaces are not perfectly clean or smooth, a direct correlation between friction and adhesion has not been established. Hence, in order to maintain generality, an a priori relationship between friction and adhesion is not assumed [33]. Therefore, work of adhesion and coefficient of friction are introduced in the analysis in an independent way. However, for particular cases where an explicit relationship between friction and adhesion can be identified, the analysis can be modified as indicated in the Appendix.
4. Strong adhesion is defined as that for which the work needed to debond the two contacting surfaces, G_{d}, is high enough to resist local debonding at the contact perimeter. The work of adhesion for receding (separating or opening) contact, G_{d}, is greater than the work of adhesion for advancing (approaching or closing) contact, w, i.e. $G_{\text{d}} > w$. Such adhesion hysteresis is due to mechanical and/or chemical effects, e.g. microplasticity of asperities [34, 35].
5. The effect of bulk and/or residual stresses in the substrate, on fatigue crack initiation, can be incorporated by superposition with the contact-induced T-stresses.
6. Finally, when certain fatigue threshold conditions are met (as described below), contact fatigue cracks are expected to initiate both in the contact pad and the flat substrate. As cracks in the contact pad are expected to be mirror images of those in the substrate across the plane of contact (i.e. they initiate at the same contact location), we discuss the stress state of the substrate only.

3.2. Three-dimensional spherical contacts

3.2.1. Normal contact fatigue. Consider a spherical pad in oscillatory normal contact with a flat substrate (Fig. 1), with the applied load, P, in the range $P_{\max} \geq P_{\min} \geq 0$. As the load decreases from its maximum, $P_{\max}$, to its minimum value, $P_{\min}$, the strain energy release rate, G, at the contact perimeter increases monotonically.

When $\max\ G < G_{\text{d}}$ or $(P_{\max} - P_{\min}) \leq 3\pi G_{\text{d}} D/4$, strong adhesion is obtained with the contact radius remaining unchanged at $a_{\max}$. The mode I cyclic stress intensity factor at the contact perimeter is given as

$$\Delta K_{\text{I}} = K_{\max} - K_{\min} = \frac{P_{\max} - P_{\min}}{2a_{\max}\sqrt{\pi a_{\max}}} \quad (14)$$

with the corresponding load ratio, $R = (\min\ K_{\text{I}}/\max\ K_{\text{I}}) = (P_{\min}/P_{\max})$.

When $\max\ G > G_{\text{d}}$ or $(P_{\max} - P_{\min}) \geq 3\pi G_{\text{d}} D/4$, weak adhesion is obtained as the work of adhesion is insufficient to sustain the singularity at the maximum contact radius, $a_{\max}$‡. Consequently, the con-

†The normal load creates a mode I stress field, as described by equations (4).

‡It is implicitly assumed in this work that debonding always occurs in a brittle and axisymmetric manner along the contact perimeter. Hence, the maximum value of G_{d} cannot be higher than the critical energy release rate for fracture of the bulk contacting materials under monotonic loading.

tact debonds at the contact perimeter and the contact radius decreases. The oscillatory mode I stress intensity factor at the contact edge, $a_{\max}$, is given as

$$\Delta K_{\mathrm{I}} = \frac{3\pi G_{\mathrm{d}} D}{8 a_{\max}\sqrt{\pi a_{\max}}} \tag{15}$$

with the corresponding load ratio, R, being

$$R = \frac{P_{\max} - (3\pi G_{\mathrm{d}} D/4)}{P_{\max}}. \tag{16}$$

As the contact conditions effectively imply a virtual circumferential crack with a circular crack front coincident with the contact perimeter [15], the initiation of a fatigue crack at the contact edge is conceptually equivalent to the onset of propagation of this pre-existing virtual crack. Hence, a fatigue crack is expected to initiate at the contact edge, $a_{\max}$, for strong or weak adhesion, if $\Delta K_{\mathrm{I}} \geq \Delta K_{\mathrm{th}}$, where ΔK_{th} is the mode I long crack initiation fatigue threshold stress intensity range for the corresponding values of R and max T.

3.2.2. Tangential fretting fatigue. Consider a sphere in contact with a planar substrate under an applied normal load $P_{\max}$ (Fig. 4). The maximum tangential load, $\bar{Q}_{\max}$, that can sustain adhesion at maximum contact radius is

$$\bar{Q}_{\max} = 2 \times \sqrt{\frac{(2-2\nu)}{(2-\nu)}\pi a_{\max}^3 \left[G_{\mathrm{d}}^{\mathrm{II}} \frac{E}{(1-\nu^2)} - \left(\frac{3 G_{\mathrm{d}}^{\mathrm{I}} \pi D}{4 a_{\max}^{3/2}} \right)^2 \right]} \tag{17}$$

where $G_{\mathrm{d}}^{\mathrm{I}}$ and $G_{\mathrm{d}}^{\mathrm{II}}$ are the critical debonding energies under pure normal and tangential loads, respectively.

If the amplitude of the applied tangential load $Q_{\max} \leq \bar{Q}_{\max}$ or equivalently the maximum energy release rate at the contact edge upon load reversal, max $G < G_{\mathrm{d}}$, then strong adhesion (stick) is obtained†.

The stress intensity factor that corresponds to the mixed mode I (steady) crack field is given by equation (5) and that which corresponds to mode II (oscillatory) crack fields at the leading and the trailing contact edges is given by

$$\Delta K_{\mathrm{II}} = \frac{Q_{\max}}{a_{\max}\sqrt{\pi a_{\max}}} \tag{18}$$

with the local effective load ratio, $R = -1$.

If the amplitude of the applied tangential load $Q_{\max} \geq \bar{Q}_{\max}$ or equivalently the maximum energy release rate at the contact edge upon load reversal, max $G > G_{\mathrm{d}}$, then weak adhesion (stick–slip) is

†The critical energy release rate, G_{d}, may depend on the mode mixity, $K_{\mathrm{I}}/K_{\mathrm{II}}$, and this could introduce a contact size effect for elastically dissimilar surfaces.

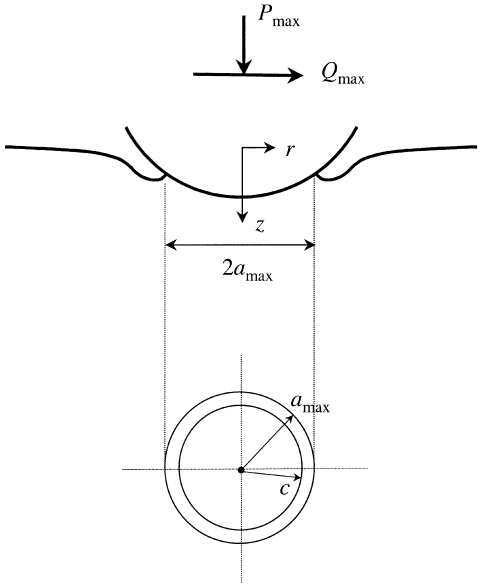

Fig. 4. Schematic illustrating tangential loading of the spherical contact.

obtained resulting in a partial slip annulus, $c \leq r \leq a_{\max}$ (Fig. 4). From global equilibrium [28]

$$Q_{\max} = \mu P_{\max}\left[1 - \left(\frac{c}{a_{\max}}\right)^3\right]; \qquad \bar{Q}_{\max} < Q_{\max} \leq \mu P_{\max}. \tag{19}$$

The tangential load that is balanced in the stick zone of radius, c, is

$$Q_{\max}^{\mathrm{in}} = Q_{\max} - \mu \frac{P_{\max}}{a_{\max}^3}(a_{\max}^2 - c^2)^{3/2}. \tag{20}$$

In this case, $K_{\mathrm{I}} = 0$, as the crack analogue predicts a closed crack-tip.

The mode II stress intensity factor at the leading and trailing edge of the stick–slip interface is given by

$$\Delta K_{\mathrm{II}} = 2 \times \min\left(\frac{Q_{\max}^{\mathrm{in}}}{2c\sqrt{\pi c}}, \quad \sqrt{\frac{G_{\mathrm{d}}^{\mathrm{II}} E}{1-\nu^2}} \right) \tag{21}$$

with the local load ratio $R = -1$.

A fatigue crack is expected to initiate, at the contact perimeter or the stick-slip boundary, for strong or weak adhesion, respectively, if the corresponding $\Delta K_{\mathrm{II}} \geq \Delta K_{\mathrm{th}}$ where ΔK_{th} is the threshold stress intensity range that corresponds to $R = -1$, and under mixed constant mode I and oscillatory mode II fatigue. This situation holds both for strong adhesion and under pure oscillatory mode II fatigue for weak adhesion.

Upon initiation, the continued propagation of the crack-tip depends on the local mode I and mode II

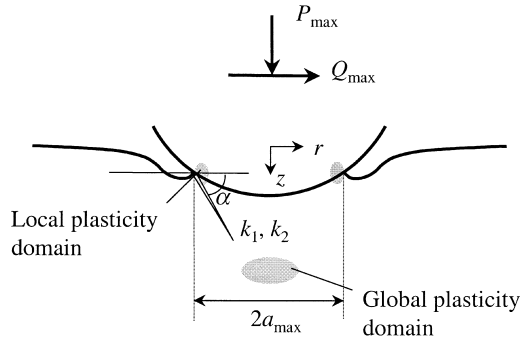

Fig. 5. Schematic illustrating crack initiation from the edge of the contact perimeter with the local crack-tip mode I and II stress intensity factors being k_1, k_2 and domains of local and global plasticity.

stress intensity factors, k_1 and k_2, respectively (Fig. 5). Following Cotterell and Rice [36], it is postulated that the crack advances in a direction along which the local mode II stress intensity factor, k_2, vanishes [or equivalently, the strain-energy release rate is maximized $(\partial/\partial\theta(k_1^2+k_2^2)=0,\ (\partial^2/\partial\theta^2(k_1^2+k_2^2)<0)$]. The initial angle of crack propagation, α, is then readily obtained from

$$k_2=\frac{1}{4}\left(\sin\frac{\alpha}{2}+\sin\frac{3\alpha}{2}\right)K_{\mathrm{I}}+\frac{1}{4}\left(\cos\frac{\alpha}{2}+3\cos\frac{3\alpha}{2}\right)K_{\mathrm{II}}=0 \tag{22}$$

at maximum load.

3.2.3. Torsional fretting fatigue. Consider a sphere in contact with a planar substrate under an applied normal load P_{max} (Fig. 3). The maximum torsional load, $\bar{M}_z$, that can sustain adhesion at maximum contact radius is

$$\bar{M}_z=\frac{4a_{max}}{3}\sqrt{\pi a_{max}^3\left[G_{\mathrm{d}}^{\mathrm{III}}\frac{E}{(1+\nu)}-\left(\frac{3G_{\mathrm{d}}^{\mathrm{I}}\pi D}{4a_{max}^{3/2}}\right)^2\right]} \tag{23}$$

where $G_{\mathrm{d}}^{\mathrm{I}}$ and $G_{\mathrm{d}}^{\mathrm{III}}$ are the critical debonding energies under pure normal and torsional loads, respectively.

If the amplitude of the applied torsional load $M_z\le\bar{M}_z$, or equivalently, the maximum energy release rate at the contact edge upon load reversal, max G < G_{d}, then strong adhesion (stick) is obtained†.

The stress intensity factor that corresponds to the mixed mode I (steady) [equation (5)] and III (oscillatory) crack fields at the leading and the trailing contact edges is given by

$$\Delta K_{\mathrm{III}}=2\sigma_{rz}^{\mathrm{tor}}\sqrt{2\pi(a_{max}-r)}=\frac{3M_z}{2a_{max}^2\sqrt{\pi a_{max}}} \tag{24}$$

with the local effective load ratio, $R=-1$.

If the amplitude of the applied tangential load, $M_z\ge\bar{M}_z$, or equivalently, the maximum energy release rate at the contact edge upon load reversal, max G > G_{d}, then weak adhesion (stick–slip) is obtained resulting in a partial slip annulus, $c\le r\le a_{max}$. A power series approximation for the relation between c/a_{max} and M_z/P_{max}, that is accurate within −3.4% error of the exact solution is given by [37]

$$\frac{M_z}{\mu P_{max}\,a_{max}}\approx k^2\left(1-\frac{3}{8}k^2-\frac{1}{64}k^4\right);\qquad k=\sqrt{1-(c/a_{max})^2}. \tag{25}$$

The torsional load that is balanced in the stick zone is

$$M_z^{\mathrm{in}}=M_z-\frac{3\mu P_{max}\,a_{max}}{8}\left(\frac{\pi}{2}-\arcsin\frac{c}{a_{max}}-\frac{c}{a_{max}}\left(2\frac{c^2}{a_{max}^2}-1\right)\sqrt{1-\frac{c^2}{a_{max}^2}}\right) \tag{26}$$

and the mode III cyclic stress intensity factor is given by

$$\Delta K_{\mathrm{III}}=2\times\min\left(\frac{3M_z^{\mathrm{in}}}{4c^2\sqrt{\pi c}},\quad\sqrt{\frac{G_{\mathrm{d}}E}{1+\nu}}\right). \tag{27}$$

In this case, $K_{\mathrm{I}}=0$, as the crack analogue predicts a closed crack-tip.

A fatigue crack is expected to initiate, at the contact perimeter or the stick–slip boundary, for strong or weak adhesion, respectively, if the corresponding $\Delta K_{\mathrm{III}}\ge\Delta K_{\mathrm{th}}$ where ΔK_{th} is the threshold stress intensity range that corresponds to $R=-1$ and $T=0$. This is valid both under mixed constant mode I and oscillatory mode III fatigue for strong adhesion, and under pure oscillatory mode III fatigue for weak adhesion.

3.3. Two-dimensional cylindrical contacts

3.3.1. Normal contact fatigue. For a cylinder of diameter, D, in adhesive contact with a flat substrate (Fig. 6) under a normal load, P_{max}, the contact width, a_{max}, is given as [5]

$$P_{max}=\frac{\pi E}{4(1-\nu^2)}\left\{\frac{a_{max}^2}{D}-2\left[\frac{4a_{max}\,w(1-\nu^2)}{\pi E}\right]\right\}. \tag{28}$$

Under an oscillatory normal load in the range $P_{max}\ge P_{min}\ge 0$, conditions for strong or weak adhesion are obtained when

†The critical energy release rate, G_{d}, may depend on the mode mixity, $K_{\mathrm{I}}/K_{\mathrm{III}}$, and this could introduce a contact size effect for elastically dissimilar surfaces.

Table 1. Adhesion-induced stress intensity factors for the case of a cylinder in oscillatory contact with a planar substrate

Loading Adhesion Mode	Normal		In-plane		Out-of-plane
	Strong-I	Weak-I	Strong-II	Weak-II	Strong-III
ΔK	$\frac{P_{\max}-P_{\min}}{\sqrt{\pi a_{\max}}}$	$\frac{3}{\sqrt{2\pi a_{\max}}}\left(\frac{G_{\mathrm{d}}^{2}\pi ED}{8(1-\nu^2)}\right)^{1/3}$	$\frac{2Q_{\max}}{\sqrt{\pi a_{\max}}}$	$2\ \min\left(\frac{Q_{\max}^{\mathrm{in}}}{\sqrt{\pi c}},\ \sqrt{\frac{G_{\mathrm{d}}E}{1-\nu^2}}\right)$	$\frac{S_{\max}-S_{\min}}{\sqrt{\pi a_{\max}}}$
R	$\frac{P_{\max}}{P_{\min}}$	$1-\frac{3}{2P_{\max}}\left(\frac{G_{\mathrm{d}}^{2}\pi ED}{8(1-\nu^2)}\right)^{1/3}$	-1	-1	-1
T-stress	max T_{xx}, max $T_{yy}=0$		max $T_{xx}=\nu$ max $T_{yy}=(2\mu P_{\max}^{*}/\pi a_{\max})$		max T_{xx}, max $T_{yy}=0$

$$(P_{\max}-P_{\min})\leq \quad \text{or} \quad >\frac{3}{2}G_{\mathrm{d}}^{2/3}\left[\frac{\pi ED}{8(1-\nu^2)}\right]^{1/3} \tag{29}$$

respectively. The corresponding stress intensity factors are summarized in Table 1.

3.3.2. In-plane fretting fatigue. When a cylindrical pad in contact with a much larger, flat substrate (Fig. 6) is subjected to an oscillatory tangential line load $Q_{\max}$ ($0\leq Q_{\max}\leq \mu P_{\max}$), under a constant normal load $P_{\max}$, the elastic energy of the cylinder becomes unbounded and the displacements are indeterminate. The solution to this problem depends critically on the overall dimensions of the fretting specimen and the applied far-field boundary conditions. Hence the precise definition for strong and weak adhesion cannot be made by the contact analysis alone.

For weak adhesion, however, the stick-zone width, c, is given from global equilibrium as

$$Q_{\max}=\mu P_{\max}\left[1-\left(\frac{c}{a_{\max}}\right)^{2}\right];\qquad 0<Q_{\max}\leq \mu P_{\max}. \tag{30}$$

Assuming adhesion is re-established at the stick zone, the tangential line load that is balanced in the stick zone is given as

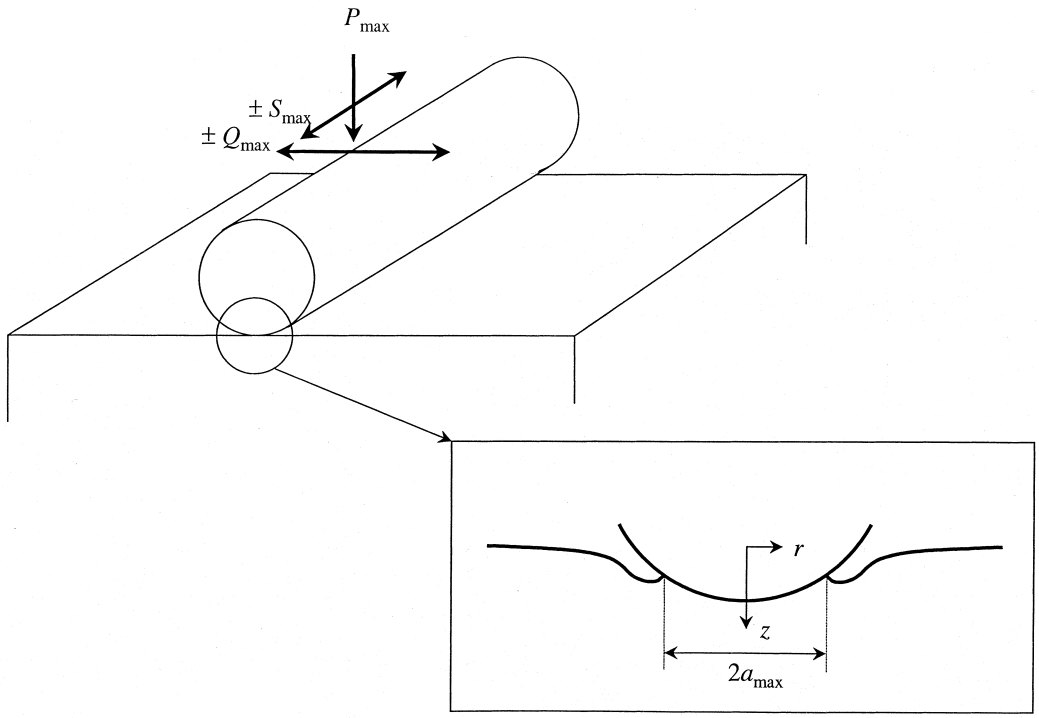

Fig. 6. Schematic illustrating loading configurations for the two-dimensional cylindrical contact geometry.

$$Q_{\max}^{\text{in}} = Q_{\max} - \frac{\mu P_{\max}}{\pi} \times \left[\frac{\pi}{2} + \arctan \frac{c\sqrt{a_{\max}^2 - c^2}}{c^2 - a_{\max}^2} - \frac{c}{a_{\max}} \left(1 - \frac{c^2}{a_{\max}^2} \right) \right]. \quad (31)$$

The corresponding stress intensity ranges for strong and weak adhesion cases are summarized in Table 1. Crack initiation is expected at the contact edge or the stick–slip boundary for strong or weak adhesion cases, respectively, when the corresponding stress intensity ranges exceed the fatigue thresholds for the corresponding R-ratios and T-stresses.

3.3.3. Out-of-plane fretting fatigue. The case of a cylinder of diameter, D, under a constant normal load, $P_{\max}$, subjected to an oscillatory line load with amplitude, $S_{\max}$, and in adhesive contact with a flat substrate (Fig. 6), can also be analyzed along similar lines and a mode III cyclic stress intensity factor range can be identified at the contact edge for strong adhesion as summarized in Table 1.

4. RANGE OF APPLICABILITY OF THE ADHESION MODEL

The preceding analysis is strictly valid under linear elastic conditions, the limits of which are defined by several criteria that predict the onset of local or global plasticity (Fig. 5), Noting that adhesion increases the effective stress under the contact area, global indentation induced plasticity can be avoided [38], provided that

$$\frac{a_{\max} E}{D\sigma_y(1-\nu^2)} < 3.675, \quad \frac{G_d E^2}{D\sigma_y^3(1-\nu^2)^2} < 7.031 \quad (32)$$

where σ_y is the yield strength of the softer of the two contacting bodies. Also, macroscopic plasticity is suppressed for $\mu > 0.25$, if [18, 24]

$$\sigma_y^3 > \frac{3P_{\max}}{2\pi a_{\max}^2} \left[\frac{(1-2\nu)^2}{3} + \frac{(1-2\nu)(2-\nu)\mu\pi}{4} + \frac{(16-4\nu+7\nu^2)\mu^2\pi^2}{64} \right]^{1/2}. \quad (33)$$

An alternative, self-consistent, Dugdale–Barenblatt model [39] for adhesive normal contact, that assumes the maximum adhesive force intensity, σ_0, to be constant until debonding is reached, whereupon it falls to zero, predicts the elastic (local, small-scale plasticity) conditions for adhesion to be preserved for

$$\sigma_0^3 \frac{D(1-\nu^2)^2}{\pi G_d E^2} > \frac{250}{9}. \quad (34)$$

The maximum adhesive stress, σ_0, could be related to the uniaxial yield strength of the cohesively weaker of the two contacting bodies, $\sigma_0 \approx 3\sigma_y$, when small-scale plasticity conditions are valid at the contact perimeter [40]. Alternately, σ_0 could be an effective stress that combines the maximum normal and the frictional shear stress [40].

Metals show appreciable adhesion at elevated temperatures and prolonged contact loading times. Under high-frequency fretting conditions, friction produces heat that raises the surface temperature and could promote creep. Therefore, for the preceding analysis to be valid, the maximum surface temperature due to tangential load oscillations must be less than a third of the homologous temperature, T_H

$$\frac{9(3\pi-4)(2-\nu)(1+\nu)}{64\pi^2 EK} \left[\frac{\mu P_{\max}}{a_{\max}} \right]^2 \Omega < \frac{T_H}{3} \quad (35)$$

where Ω is the fretting frequency and K is the thermal conductivity coefficient [41].

Another limitation of the present analysis comes from the surface morphology. Surface roughness diminishes the influence of adhesion if [42]

$$\left[\frac{3(1-\nu^2)}{2E} \right]^2 \geq 100 \frac{G_d^2 \rho_0}{\Sigma^3} \quad (36)$$

where Σ is the standard deviation of the microasperity heights and ρ_0 is the average radius of curvature of the asperity tips.

5. EXPERIMENTAL VALIDATION OF THE ANALYSES

In comparing various experiments to model predictions, only reasonable estimates are chosen from the empirical relationship [equation (A1)] that relates the friction coefficient to the debond energy, since experimentally measured values for the debond energy are not available.

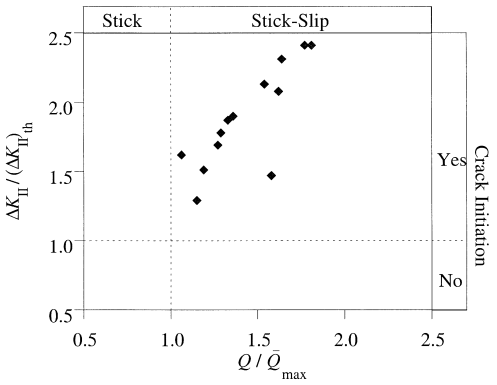

Fig. 7. Room temperature fretting fatigue experiments on Al-7075 T6 (with in 2 in. diameter sphere on flat geometry) (see Ref. [22] and current work), evaluated using the present adhesion model where in the mode II threshold stress intensity factor for an R-ratio of -1 was estimated to be ≈ 1 MPa $m^{1/2}$ and the work of adhesion for advancing and receding contacts (w, G_d) being ≈ 1 and ≈ 19 N/m, respectively.

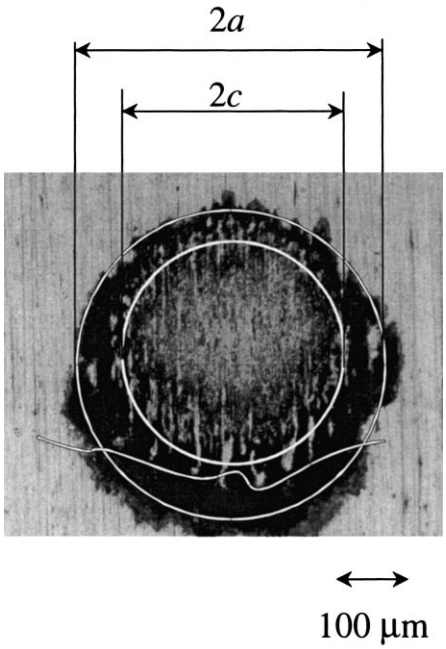

Fig. 8. Fretting scar produced on the flat Al-7075 T6 substrate [22] when fretted with a spherical pad of the same material and diameter 2 in., for $P_{max}=20$ N, $Q_{max}=15$ N and an axial stress of 59 NPa with an R-ratio $=-1$ indicating that cracks initiate near the stick–slip boundary.

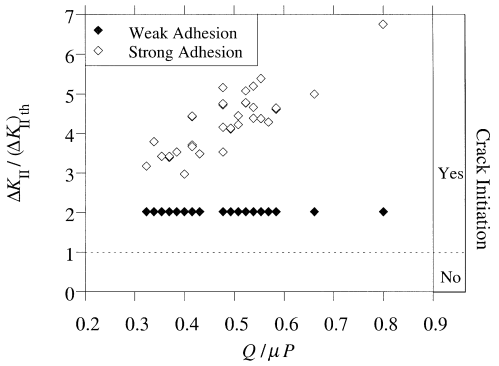

Fig. 9. Room temperature fretting fatigue experiments on Al-2024 T351 (with a 0.5 in. diameter cylinder on flat geometry [50]) evaluated using the present adhesion model where in the mode II threshold stress intensity factor for an R-ratio of -1 was estimated to be $\approx$1 MPa m$^{1/2}$ and the work of adhesion for advancing and receding contacts (w, G_d) being $\approx$1 and $\approx$12 N/m, respectively.

5.1. Three-dimensional spherical contacts

Room temperature tangential fretting fatigue experiments, using a set-up described in detail in Ref. [43], were performed by Wittkowsky *et al.* [22] on 7075 T6 aluminum alloy, with mechanical properties, $E=71.5$ GPa, $\nu=0.33$, $\sigma_y=483$ MPa, and threshold $\Delta K_{II}=1$ MPa m$^{1/2}$, and the experimentally determined friction coefficient, $\mu=1.2$. Using reasonable values for the work of adhesion for advancing and receding contacts, $w=1$ N/m and $G_d=19$ N/m [from equation (A1)], the adhesion model predicts weak adhesion, in agreement with experiments where in all cases, stick–slip behavior was observed. The conditions (Fig. 7) and location of crack initiation (stick–slip boundary, Fig. 8) are also predicted well by the model. While the model predicts an initial crack angle of 70.5°, crack initiation angles ranging between 61° and 80° were observed experimentally. Some deviations from model predictions are expected as the material grain size of 60μm was comparable to the stick–slip zone size in many cases, while the model is strictly valid under conditions of complete material homogeneity and isotropy.

Also, as summarized in Table 2, fretting fatigue experiments on a variety of other material systems can be interpreted within the context of adhesion. Conditions of strong and weak adhesion can be identified and, in a number of cases, the observed location of crack initiation agrees with the model predictions, as shown in Table 2.

Table 2. Experimental observations on contact fatigue crack initiation[a]

Material	D_{eff} (mm)	P_{max} (N)	P_{min} (N)	Q (N)	M (Nm)	μ	$\bar{P}_{max}$ (N), $\bar{Q}_{max}$ (N), $\bar{M}_z$ (N m)	Adhesion	ΔK_{model} (MPa m$^{1/2}$)	ΔK_{th} (MPa m$^{1/2}$)	Cracking predicted (observed)	Location		Ref.
												Predicted	Observed	
En31 steel	10.16	1537	170	0	0	0.8	0.9	Weak	0.02	2–5	No (Yes)	–	Surface	[44]
Hard steel	63.5	127,400	4900	0	0	0.8	6.0	Weak	0.004	2–5	No (Yes)	–	Edge	[45]
SAE 52100 steel	12.7	88	88	0	0.009	0.8	0.001	Weak	2.5	2–5	Yes (Yes)	Stick–slip	Surface	[46]
Al-7075	600	1000	1000	930	0	1.2	296	Weak	2.4	1	Yes (Yes)	Stick–slip	Edge, stick–slip	[20, 21]
Al-7075 T7351	1000	500	500	525	0	1.2	252	Weak	2.4	1	Yes (Yes)	Stick-slip	Edge, stick–slip	[47]
Ti–6Al–4V	300	700	700	525	0	0.8	152	Weak	2.1	2	Yes (Yes)	Stick–slip	Edge	[47]
Ti–6Al–4V	8	100	100	70	0	0.8	9	Weak	2.1	2	Yes (Yes)	Stick–slip	Edge	[13]
Nb	6.25	10.9	10.9	10	0	1.0	2.8	Weak	2.3	–	– (Yes)	–	Stick–slip	[49]

[a] In all cases, sphere on flat geometry was used, except for Nb where a cylinder on cylinder point contact was established. D_{eff}: the effective diameter of the contacting sphere; P_{max}: maximum normal load; P_{min}: minimum normal load; Q: tangential load amplitude; M:torsional load amplitude; $\bar{P}_{max}$ $\bar{Q}_{max}$ $\bar{M}_z$: critical normal, tangential or torsional loads above which weak adhesion is obtained; ΔK_{model}: stress intensity factor range predicted by the adhesion model; ΔK_{th}: material fatigue threshold stress intensity factor range for load ratio $R=-1$ (estimated from Ref. [48]); Surface: contact surface; Edge: edge of the contact; Stick–slip: stick–slip boundary.

5.2. Two-dimensional cylindrical contacts

For the tangential fretting fatigue studies on 2024–T351 aluminum reported in Ref. [50], with material properties, $E = 74.1$ GPa, $\nu = 0.33$, $\mu = 0.65$, and using threshold $\Delta K_{II} = 1$ MPa $m^{1/2}$, $w = 1$ N/m and $G_d = 12$ N/m, the cyclic mode II stress intensity factors predicted by the model are greater than the fatigue threshold for $R = -1$, in agreement with the observation of crack initiation in all the reported experiments (Fig. 9). While dominant fatigue cracks were located at the contact edge, cracks were also observed at the stick–slip boundary. This indicates a possible transition from an initial strong adhesion stage to a final weak adhesion stage.

In fretting fatigue studies on 0.34% carbon steel [51], adhesion was identified as a precursor to the contact edge cracks that initiated under very low tangential load amplitude. This indicates strong adhesion in the context of the present analysis.

When a cylinder on cylinder line contact system was subjected to oscillatory oblique force loading, two type of cracks, one at the contact edge and the second at the stick–slip boundary were observed [52]. The adhesion model can explain this phenomenology by recognizing that the equivalent normal and tangential load oscillations can initiate cracks at the contact edge and the stick–slip boundary, respectively.

In addition, the adhesion model can qualitatively predict the observed cracking pattern reported by Dawson [45] for normal load contact fatigue tests with cylindrical pads while conventional contact mechanics analysis cannot do so as it predicts a fully compressive stress field. However, a rigorous quantitative comparison is not attempted here as substantial plasticity was observed in these experiments.

6. CONCLUSIONS

The present work examined the role of adhesion in contact mechanics with a particular emphasis on fatigue crack initiation for a variety of contact geometries (sphere or cylinder on a flat substrate) and loading conditions (constant or oscillatory normal, tangential or torsional).

It was demonstrated that:

- The adhesion-induced, square-root singular stress fields could be analyzed within the framework of a "crack analogue" and hence the pre-existing, virtual long crack introduced by the contact circumvents "length scale" problems inherent in the modeling of crack initiation based on conventional fracture mechanics;
- Under adhesive normal, tangential or torsional contact loading conditions, mode I, II or III stress intensity factors could be identified at the contact perimeter or at the stick–slip boundary for strong or weak adhesion, respectively;
- By comparing to the material fatigue thresholds, contact conditions required for crack initiation could be predicted. Additionally, the location and initial crack propagation directions could also be predicted, in reasonable agreement with experimental results.

Under conditions of small-scale yielding, the effects of static and/or oscillatory bulk stresses acting parallel to the contact surface (such as the far-field applied or residual stresses arising from surface modification treatments due to shot-peening or laser shock-peening) can be analyzed by recognizing that these are analogous to the T-stresses present in a linear elastic fatigue–fracture formulation. The propensity for contact fatigue crack initiation could be suppressed by selecting material or environmental combinations that effectively reduce adhesion in a contact system.

Acknowledgements—This work was supported by the Multi-University Research Initiative on "High Cycle Fatigue", which is funded at MIT by the Air Force Office of Scientific Research, Grant No. F49620-96-1-0278, through a subcontract from the University of California at Berkeley.

REFERENCES

1. Johnson, K. L., *Contact Mechanics*. Cambridge University Press, Cambridge, 1985.
2. Johnson, K. L., *Proc. R. Soc. Lond.*, 1954, **A230**, 531.
3. Johnson, K. L., Kendall, K. and Roberts, A. D., *Proc. R. Soc. Lond.*, 1971, **A324**, 301.
4. Pollock, H. M., Maugis, D. and Barquins, M., *App. Phys. Lett.*, 1978, **33**, 798.
5. Kalker, J. J., *Wear*, 1987, **119**, 63.
6. Savkoor, A. R. and Briggs, G. A. D., *Proc. R. Soc. Lond.*, 1977, **A356**, 103.
7. Bethune, B. and Waterhouse, R. B., *Wear*, 1965, **8**, 22.
8. Bethune, B. and Waterhouse, R. B., *Wear*, 1968, **12**, 289, 369.
9. Sato, J., Shima, M. and Suguwara, T., *Wear*, 1985, **106**, 53.
10. Higham, P. A., Bethune, B. and Stott, F. H., *J. Mater. Sci.*, 1977, **12**, 2503.
11. Burton, R. A. and Russell, J. A., *J. Basic Engng*, 1966, **88**, 573.
12. Malkin, S., Majors, D. P. and Courtney, T. H., *Wear*, 1972, **22**, 235.
13. Koenen, A., Virmoux, Ph, Gras, R., Blouet, J., Dewulf, J. M. and De Monicault, J. M., *Wear*, 1996, **197**, 192.
14. Waterhouse, R. B., *Wear*, 1977, **45**, 355.
15. Giannakopoulos, A. E., Lindley, T. C. and Suresh, S., *Acta mater.*, 1998, **46**, 2955.
16. Cheng, W., Cheng, H. S., Mura, T. and Keer, L. M., *ASME Trans. J. Tribology*, 1994, **116**, 2.
17. Hills, D. A., *Wear*, 1994, **173**, 107.
18. Hamilton, G. M., *Proc. Inst. Mech. Engrs*, 1983, **197C**, 53.
19. Fouvry, S., Kapsa, Ph, Vincent, L. and Dang Van, K., *Wear*, 1996, **195**, 21.
20. Lamacq, V., Dubourg, M.-C. and Vincent, L., *J. Tribology*, 1996, **118**, 711.
21. Lamacq, V., Dubourg, M.-C. and Vincent, L., *Tribology Int.*, 1997, **30**, 391.

22. Wittkowsky, B. U., Birch, P. R., Dominguez, J. and Suresh, S., in *Fretting Fatigue: Current Technology and Practices*, ed. D. W. Hoeppner, Chandrasekaran and C. B. Elliot. American Society for Testing and Materials, 1999, ASTM STP 1367.
23. Semenchenko, V. K., *Surface Phenomena in Metals and Alloys*. Addison-Wesley, Reading, MA, 1962.
24. Barquins, M. and Maugis, D., *J. Mec. Theor. Appl.*, 1982, **1**, 331.
25. Maugis, D. and Barquins, M., *J. Phys. D: Appl. Phys.*, 1978, **11**, 1989.
26. Greenwood, J. A. and Johnson, K. L., *Phil. Mag.*, 1981, **43**, 697.
27. Williams, M. L., *Bull. Seismol. Soc. Am.*, 1959, **49**, 199.
28. Mindlin, R. D., *J. Appl. Mech*, 1949, **16**, 259.
29. Westmann, R. A., *J. Appl. Mech.*, 1965, **87**, 411.
30. Bowden, F. P. and Tabor, D., *Friction and Lubrication of Solids, Part I*. Oxford University Press, London, 1950.
31. Bowden, F. P. and Tabor, D., *Friction and Lubrication of Solids, Part II*. Oxford University Press, London, 1964.
32. McFarlane, J. S. and Tabor, D., *Proc. R. Soc. Lond.*, 1950, **A202**, 244.
33. Bikerman, J. J., *Wear*, 1976, **39**, 1.
34. Chowdhury, S. K. R., Hartley, N. E. W., Pollock, H. M. and Wilkins, M. A., *J. Phys. D: Appl. Phys.*, 1980, **13**, 1761.
35. Chowdhury, S. K. R. and Pollock, H. M., *Wear*, 1981, **66**, 307.
36. Cottrell, B. and Rice, J. R., *Int. J. Fract.*, 1980, **16**, 155.
37. Deresiewicz, H., *J. Appl. Mech.*, 1954, **76**, 52.
38. Maugis, D. and Pollock, H. M., *Acta Metall.*, 1984, **32**, 1323.
39. Maugis, D., *J. Colloid Interface Sci.*, 1992, **150**, 243.
40. Johnson, K. L., *Langmuir*, 1996, **12**, 4510.
41. Greenwood, J. A. and Alliston-Greiner, A. F., *Wear*, 1992, **155**, 269.
42. Fuller, K. N. G. and Tabor, D., *Proc. R. Soc. Lond.*, **A345**, 327
43. Wittkowsky, B. U., Birch, P. R., Dominguez, J. and Suresh, S., *Fatigue Fract. Engng Mat. Str.*, 1999, **22**(4), 307.
44. Kennedy, N. G., *Proc. Int. Conf. Fatigue of Metals*, London. I. Mech. E., ASME, 1956, p. 282.
45. Dawson, P. H., *J. Mech. Engng Sci.*, 1967, **9**, 67.
46. Kennedy, P. J., Stallings, L. and Peterson, M. B., *ASLE Trans.*, 1983, **27**, 305.
47. Blanchard, P., Colombie, Ch, Pellerin, V., Fayeulle, S. and Vincent, L., *Metall. Trans.*, 1991, **22A**, 1535.
48. Suresh, S., *Fatigue of Materials*, 2nd ed. Cambridge University Press, Cambridge, 1998.
49. Bryggman, U. and Soderberg, S., *Wear*, 1988, **125**, 39.
50. Szolwinski, M. P. and Farris, T. N., *Wear*, 1998, **221**, 24.
51. Endo, K. and Goto, H., *Wear*, 1976, **38**, 311.
52. Yashamita, N. and Mura, T., *Wear*, 1983, **91**, 235.

APPENDIX

An empirical relation between adhesion and friction of metal surfaces and a spherical indenter based on micro-plasticity of the asperities under shear and normal loading was derived in Ref. [32]. Using the smallest normal load and the sphere diameter used in their experiments, their empirical equation can be stated in terms of critical debonding energy release rate, G_d, as

$$G_d = 14.3651\sqrt{0.3 + \mu^2}\ \text{(N/m)}. \tag{A1}$$

As an example, for $\mu = 1$, $G_d = 16$ N/m.